Geoscience Frontiers 13 (2022) 101425

HOSTED BY

Contents lists available at ScienceDirect

Geoscience Frontiers

journal homepage: www.elsevier.com/locate/gsf

Research Paper

Multi-hazard susceptibility mapping based on Convolutional Neural Networks

Kashif Ullah [a], Yi Wang [a,b,*], Zhice Fang [a], Lizhe Wang [b,c,d], Mahfuzur Rahman [e]

[a] Institute of Geophysics and Geomatics, China University of Geosciences, Wuhan 430074, China
[b] State Key Laboratory of Biogeology and Environmental Geology, China University of Geosciences, Wuhan 430074, China
[c] School of Computer Science, China University of Geosciences, Wuhan 430074, China
[d] Hubei Key Laboratory of Intelligent Geo-Information Processing, China University of Geosciences, Wuhan 430074, China
[e] Department of Civil Engineering, International University of Business Agriculture and Technology (IUBAT), Dhaka 1230, Bangladesh

ARTICLE INFO

Article history:
Received 27 January 2022
Revised 5 May 2022
Accepted 15 June 2022
Available online 17 June 2022
Handling Editor: B. Pradhan

Keywords:
Multi-hazard
Convolutional Neural Network
Machine learning
Eastern Hindukush
Pakistan

ABSTRACT

Multi-hazard susceptibility prediction is an important component of disasters risk management plan. An effective multi-hazard risk mitigation strategy includes assessing individual hazards as well as their interactions. However, with the rapid development of artificial intelligence technology, multi-hazard susceptibility prediction techniques based on machine learning has encountered a huge bottleneck. In order to effectively solve this problem, this study proposes a multi-hazard susceptibility mapping framework using the classical deep learning algorithm of Convolutional Neural Networks (CNN). First, we use historical flash flood, debris flow and landslide locations based on Google Earth images, extensive field surveys, topography, hydrology, and environmental data sets to train and validate the proposed CNN method. Next, the proposed CNN method is assessed in comparison to conventional logistic regression and *k*-nearest neighbor methods using several objective criteria, i.e., coefficient of determination, overall accuracy, mean absolute error and the root mean square error. Experimental results show that the CNN method outperforms the conventional machine learning algorithms in predicting probability of flash floods, debris flows and landslides. Finally, the susceptibility maps of the three hazards based on CNN are combined to create a multi-hazard susceptibility map. It can be observed from the map that 62.43% of the study area are prone to hazards, while 37.57% of the study area are harmless. In hazard-prone areas, 16.14%, 4.94% and 30.66% of the study area are susceptible to flash floods, debris flows and landslides, respectively. In terms of concurrent hazards, 0.28%, 7.11% and 3.13% of the study area are susceptible to the joint occurrence of flash floods and debris flow, debris flow and landslides, and flash floods and landslides, respectively, whereas, 0.18% of the study area is subject to all the three hazards. The results of this study can benefit engineers, disaster managers and local government officials involved in sustainable land management and disaster risk mitigation.

1. Introduction

Environmental hazards are usually studied separately. Many researchers around the world focus on single hazards, such as landslides (Wang et al., 2020a; Habumugisha et al.,2022; Youssef et al.,2022a), floods (Hosseini et al., 2021; Rafiei-Sardooi et al., 2021), debris flows (Marra et al., 2017; Abuzied and Pradhan, 2021), forest fires (Abedi Gheshlaghi et al., 2021; Feizizadeh et al., 2022), and glacier avalanches (Choubin et al., 2019; Yariyan et al.,2022). However, many locations are susceptible to multiple hazards, which may occur simultaneously or as cascading events. Mitigating one hazard may exacerbate the frequency,

Abbreviations: LSM, Landslide Susceptibility Mapping; FFSM, Flash Flood Susceptibility Mapping; DFSM, Debris Flow Susceptibility Mapping; CNN, Convolutional Neural Network; DL, Deep Learning; MCDM, Multi-Criteria Decision-Making; ML, Machine Learning; LR, Logistic Regression; KNN, K-Nearest Neighbor; SPI, Stream Power Index; NDVI, Normalized Difference Vegetation Index; STI, Sediment Transportation Index; NDMA, National Disaster Management Authority; TWI, Topographic Wetness Index; ALOS, Advanced Land Observing Satellite; DEM, Digital Elevation Model; AUC, Area Under the Receiver Operating Characteristic Curve; OA, Overall Accuracy; MAE, Mean Absolute Error; RMSE, Root Mean Square Error; PCC, Pearson Correlation Coefficient; MDG, Mean Decrease Gini.

* Corresponding author.
E-mail addresses: Kashif@cug.edu.cn (K. Ullah), cug.yi.wang@gmail.com (Y. Wang), zhicefang@cug.edu.cn (Z. Fang), lzwang@cug.edu.cn (L. Wang), mfz.rahman@iubat.edu (M. Rahman).

https://doi.org/10.1016/j.gsf.2022.101425
1674-9871/

duration, distribution, or intensity of another hazard, especially in the mountainous regions (Kappes et al., 2012; Pourghasemi et al., 2020; Pouyan et al., 2021).

Pakistan is a disaster-prone country in South Asia, having suffered about $18 billion in damage and losses over the past few decades (Ullah et al., 2020; Ali et al., 2021). Flash floods, debris flows, and landslides are the most prevalent natural disasters in mountainous Karakoram Hindukush in Pakistan (Wasson, 1978; Shaw, 2015; Ali et al., 2021; Hussain et al., 2021). As a disaster-prone country with high exposure to hydrometeorological and geological disasters damages caused by floods, landslides, and debris flows are increasing due to climate change and uncontrolled development (Ullah and Zhang, 2020). Between 1970 and 2010, more than 90,000 people have died due to disasters (Ullah et al., 2020; Ullah and Zhang, 2020). Disaster-related losses have calculated more than $20 billion, including $10 billion in losses from the 2010 flood and $5 billion from the 2005 earthquake and earthquake-induced landslides (Downton et al., 2005; Bronkhorst, 2012; Khan et al., 2021). During the monsoon season (July–September), heavy rainfall triggered flash floods, landslides, and debris flows in the Karakorum Hindukush region of Pakistan, resulting in casualties and property losses. Together, these risks cause serious damage to the road network and unfavorable environmental conditions, and endanger human health and well-being (Pourghasemi et al., 2019; Yousefi et al., 2020). Although it is challenging to prevent debris flows, flash floods and landslides, the distribution map of their occurrence can be drawn to identify probabilities and potential risks (Skilodimou et al., 2019; Liu et al., 2020; Yousefi et al., 2020; Azareh et al., 2021; Li et al., 2021). In this regard, multi-hazard probability mapping is a key step to determine the likelihood of potential hazards. Multi-hazard probability mapping is the first step of comprehensive risk assessment and quantification (Pourghasemi et al., 2019; Rahmati et al., 2019). In addition, probability mapping can help disaster managers and other authorities better prepare for and mitigate losses (Corominas et al., 2014; Pourghasemi et al., 2019).

The United Nations (UN) has adopted the term of multi-hazard in the framework of sustainable development goals and agenda 21 to reduce disaster risk (UNEP, 1992; Pourghasemi et al., 2020). Multi-hazard risk assessment is inseparable from the long-term sustainable development of society (Uitto and Shaw, 2016). Globally, the scale and frequency of multi-hazard damage are increasing (Lombardo et al., 2020). Policymakers and engineers require knowledge on multi-hazard risk zones for site selection to support socio-economic development and sustainable management of natural resources (Bathrellos et al., 2017).

Although multi-hazard research has become more and more common in recent decades (Pourghasemi and Kerle, 2016; Skilodimou et al., 2019; Sanam et al., 2020), there are still challenges facing scientists in the 21st century (UN, 2002). Various methods have been used to assess the probability of multi-hazards using GIS and RS technologies (Ali et al., 2021; Rahman et al., 2021; Segoni and Caleca, 2021). In addition, multi-criteria decision-making (MCDM), machine learning (ML), and hybrid machine learning approaches are also used to draw multi-hazard maps in various parts of the world (Furlan et al., 2018; Mafi-Gholami et al., 2019; Skilodimou et al., 2019; Aksha et al., 2020; Cao et al., 2020; Lombardo et al., 2020; Mosavi et al., 2020; Nachappa et al., 2020; Pourghasemi et al., 2020; Yanar et al., 2020; Pouyan et al., 2021; Rahman et al., 2021). ML methods are more suitable for finding data relationships between hazard and causative factors than traditional statistical methods and MCDM (Huang et al., 2020). However, with rapid advancement in research, it was found that traditional ML models directly classify the natural hazard data and fail to recognize hidden relationship that exists in the data, ultimately failing to further improve classification accuracy (Wang et al., 2019).

To address this problem, another branch of ML known as Deep Learning (DL) has emerged as one of the best methods because it can solve the targeted problems more effectively than traditional ML methods (Wang et al., 2019). Precisely, DL approaches have advanced dramatically in recent years, particularly in image interpretation (Wang et al., 2020a; Azarafza et al., 2021; Dikshit and Pradhan, 2021). Besides, these may be useful in understanding the performance of multi-hazards susceptibility models because of their more sophisticated algorithmic structure (Dikshit et al., 2021). However, there is a divergence of opinion regarding the selection of a suitable method for mapping multi-hazard prone areas, particularly in data-poor countries like Pakistan. Convolutional Neural Network (CNN) is a popular DL technique which has demonstrated superior performance in many image processing tasks (Simard et al., 2003; Wang et al., 2019, 2020a). Compared to traditional ML algorithms, the CNN framework contains convolutional and subsampling layers. As a result, CNN requires fewer parameters and allows more efficient mining of latent relationships in data (Yi et al., 2020). Specifically, CNN has achieved outstanding results in image classification due to convolutional and subsampling layers, which can effectively extract hidden information from an image (Wang et al., 2020a; Yi et al., 2020). In recent years, CNN has been used for single environmental hazard susceptibility mapping, i.e., floods, landslides, debris flows and forest fire susceptibility mapping, and has demonstrated higher predictive capabilities than conventional machine learning algorithms (Wang et al., 2019, 2020a; Zhang et al., 2019; Chen et al., 2020; Fang et al., 2020; Youssef et al.,2022a,b). However, DL methods have not been used to explore the potential of improvements on multi-hazard susceptibility mapping.

This study aims to provide a regional multi-hazard (flash floods, debris flows, and landslides) susceptibility prediction framework based on CNN for the mountainous region district Shangla, eastern Hindukush, Pakistan. To the best of our knowledge, this is the first attempt to investigate the feasibility of CNNs with powerful prediction performance for multi-hazard susceptibility prediction in the study area of eastern Hindukush, Pakistan. To date, only a limited number of studies has been conducted to investigate multi-hazards, which is extremely evident in developing countries. The aim of this study is to address the gap in the literature. Therefore, it is considered beneficial for multi-hazard susceptibility modeling to implement the proposed method. Moreover, to evaluate the effectiveness of our CNN-based framework, we compare it with conventional LR and KNN models using several statistical measures. Notably, the proposed method can be used for any environmental hazard, not only the aforementioned three hazards. Thus, this study introduces a tool for the sustainable management of emergencies in pre-and-post-multi-hazards scenarios.

2. Study area and available data

2.1. Study area

As shown in Fig. 1, the study area is located in Shangla District, eastern Hindu Kush region of Pakistan, with an area of about 1586 km^2, and in the tropical sub-humid zone (Hussain et al., 2021). The study area's altitude ranges from 391 m in the south to more than 4000 m in the north; the highest peaks are Bera Charai and Chapere Sar, at 2850 m and 3590 m, respectively. During the summer monsoons, there is heavy rainfall and snowfall at high altitudes, and the average annual precipitation is between 1200 mm and 1600 mm (Atta-Ur-Rahman and Shaw, 2015;

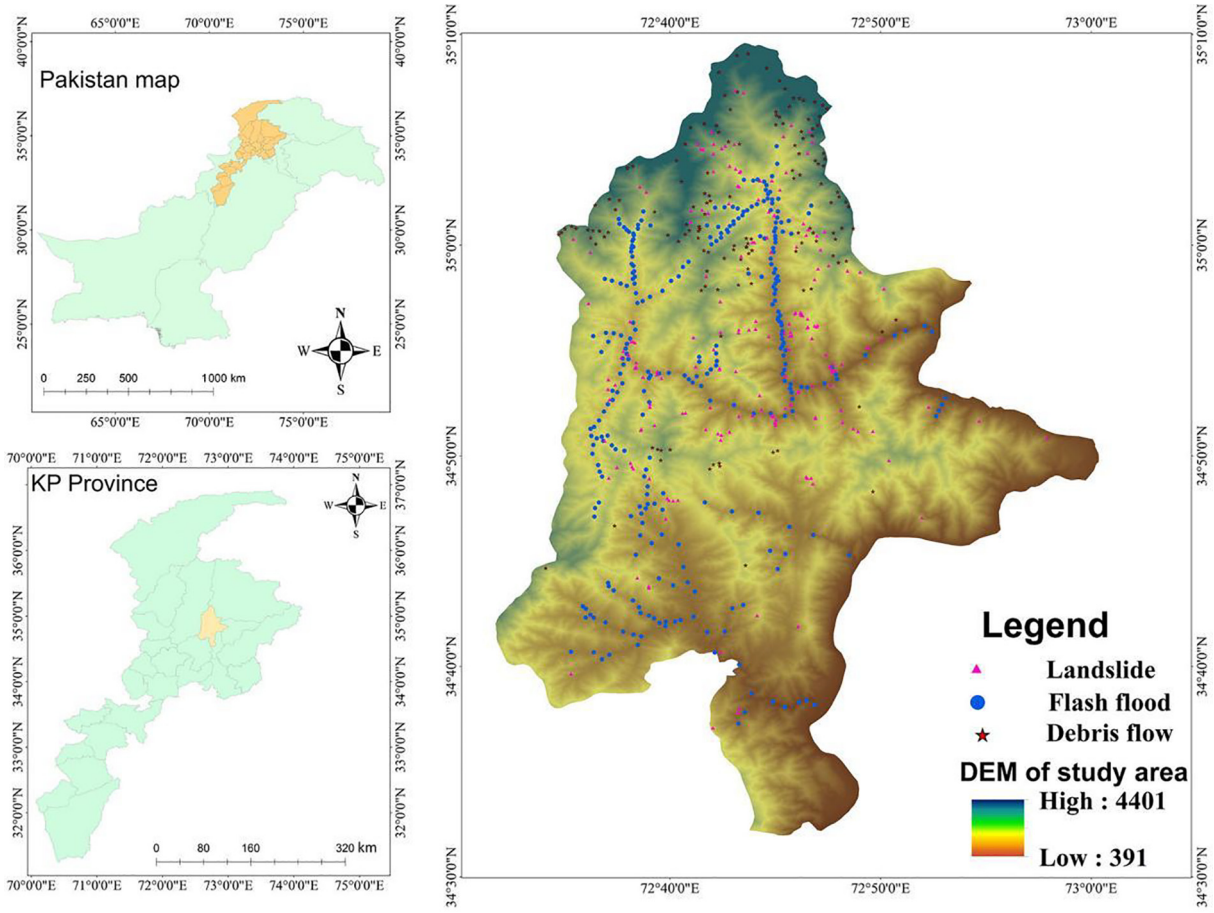

Fig. 1. Location of the study area.

Hussain et al., 2021). Geologically, the area consists of rocks of various ages. The topography is the result of the collision of the Indian and Eurasian plates. The Hindu Kush Mountains and the Pamirs form most seismically active intermediate-depth seismic zone in the world. In addition, the area is composed of rocks of different ages, including Cretaceous rocks composed of granite and gneiss, Mesozoic rocks composed of mélange and marble green, Phyl rocks, Precambrian quartzite phyllite and schist, and Paleozoic rocks composed of schist and marble facies.

For decades, the study area has suffered from earthquakes, landslides, debris flows, flash floods, and many other environmental disasters, causing severe casualties and land degradation. Fig. 2 illustrates field photos of landslide, flash flood, and debris flow in the study area.

2.2. Multi-hazard inventories and causative factors

Hazard inventories are important in susceptibility mapping (Ullah and Zhang, 2020; Rahman et al., 2021), and in establishing relationships between a hazard and variables that cause it (Song et al., 2020). Based on the disaster reports of various government organizations and forest departments and non-governmental organizations, three types of hazards were considered in this study: landslides, flash floods, and debris flow. Flood and debris flow sus-

Fig. 2. Field photos of different hazards. (a) Landslide, (b) flash flood, (c) debris flow.

ceptibility assessment is very similar to the landslide susceptibility mapping (LSM) method. In terms of sampling, two sampling strategies have been widely used. The first method is to draw polygons from prominent steep slopes, and the second method is point sampling, where the sampling points are recorded at the site of the landslide occurrence (Dou et al., 2020). Although each sampling strategy has advantages and disadvantages, the main principle is that the sampling strategy applied should fit to the study area.

This study established a multi-hazard inventory of three hazards based on NDMA data, interpretation of multi-temporal high-resolution images from 2000 to 2020 using Google Earth, and field observations. In the Multi-hazard inventory map, sampling points typically represent areas affected by historical Multi-hazard (Pourghasemi et al., 2020). It should be noted that the debris flow and flood-affected areas were identified as sampling points for FSM in several previous studies (Pourghasemi et al., 2020; Ullah and Zhang, 2020; Wang et al., 2020a,b). According to the literature, the inventory was randomly divided into training and testing datasets. Among them, 70% of the data were used to train the model, and the remaining 30% data were used to verify the results.

According to the existing literature and the environmental characteristics of the study region, we selected 15 causative factors for analysis shown in Fig. 3 and Table 1, of which 12 were used to assess flash floods, 14 were used for debris flows and 13 were used for landslides. All topographic factors, namely elevation, slope, distance to rivers, aspect, plan and profile curvature, topographic wetness index (TWI), stream power index (SPI), and sediment transportation index (STI), were derived from ALOS digital elevation model (DEM) data and a brief description of all causative factors is given below.

Table 1
Multi-hazard causative factors for each hazard.

Factors	Flash flood	Landslide	Debris flow
Slope angle	✓	✓	✓
Elevation	✓	✓	✓
Plan curvature	✓	✓	✓
Profile curvature	–	✓	✓
Geology	✓	✓	✓
Distance to faults	–	✓	–
Distance to roads	✓	✓	✓
Distance to streams	✓	✓	✓
SPI	✓	–	✓
STI	✓	–	✓
TWI	✓	✓	✓
NDVI	–	✓	✓
Landcover	✓	✓	✓
Mean annual rainfall	✓	✓	✓
Aspect	✓	✓	✓

2.2.1. Elevation

Elevation is one of the most essential factors in assessing natural hazards (Aksha et al., 2020; Bui et al., 2020; Chen et al., 2020). Flood, landslide, and debris flow frequency can all be influenced by elevation. Flood water often inundates at low elevation, although

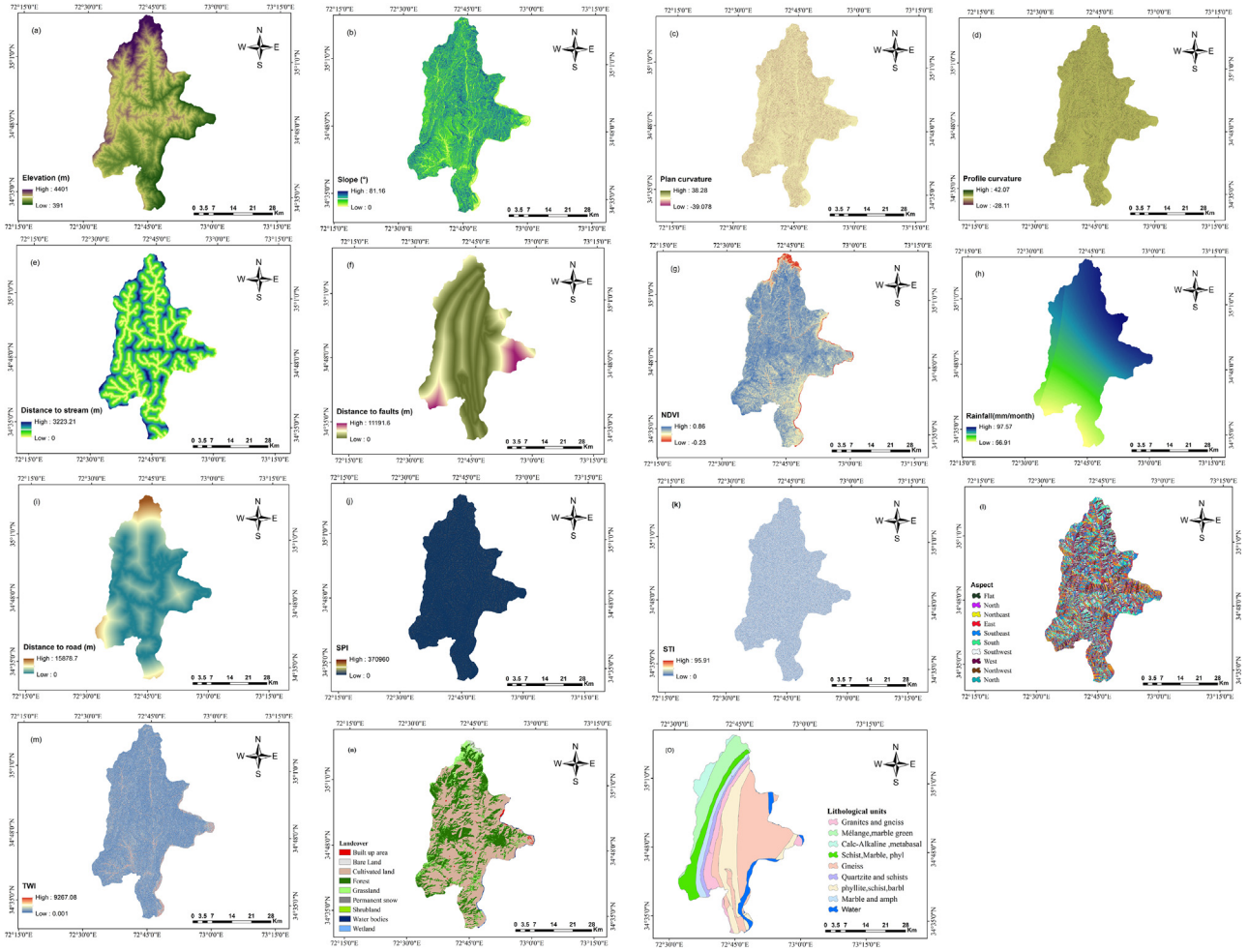

Fig. 3. Multi-hazard causative factors considered in this study.

debris flow and landslide risk are minimal at low elevation due to the gentle slope; nevertheless, susceptibility to debris flow and landslide is significant at medium and high elevation due to the gentle slope (Fig. 3a).

2.2.2. Slope

The slope angle significantly impacts on debris flow, flash flooding, and landslides (Wang et al., 2020a,b; Li et al.,2021). Flooding is common in flat areas due to water inundation, and steep slope areas are more prone to slope destabilization, resulting in debris flow and landslides (Fig. 3b).

2.2.3. Profile and plan curvatures

Curvature is used to convey information about the topographical shape of a region (Oh and Pradhan, 2011; Das, 2019). The profile curvature specified the highest slope, and the plan curvature defined the contour curvature of a region (Fang et al., 2021) (Fig. 3c, d).

2.2.4. Distance to streams

Distance to streams is another critical factor in estimating debris flow, flood and landslide (Khosravi et al., 2016; Chen et al., 2020; Mandal et al., 2021). Heavy rainfall areas adjacent to rivers exacerbate flooding due to water accumulation (Das, 2019). Stream erosion can destabilize the slope and can alter landslide and debris flow by wetting low low-lying slopes (Chen et al., 2020) (Fig. 3e).

2.2.5. Lithology and distance to faults

Lithological units and distance to faults are essential to define the debris flows and landslides in each location (Pourghasemi and Kerle, 2016; Chen et al., 2020; Fang et al., 2021). The lithological map and fault lines were digitized from the 1:100,000 scale geological map of Khyber Pakhtunkhwa Province obtained from the Geological Survey of Pakistan, as shown in (Table 2 and Fig. 3f, o).

2.2.6. The normalized difference vegetation index (NDVI)

NDVI has been extensively used to assess the degree of vegetation development on slopes and its impact on runoff, infiltration, and weathering. Hence, NDVI is always a significant feature to reflect vegetation characteristics in a landslide, flash flood, and debris flow susceptibility mapping (Chen et al., 2017; Wang et al., 2020a; Fang et al., 2021). NDVI was derived from a sentinel-2 satellite image using the Eq. (1) in ArcGIS v.10.6,

$$\mathrm{NDVI} = \frac{\mathrm{B8} - \mathrm{B4}}{\mathrm{B8} + \mathrm{B4}} \tag{1}$$

where B4 is for the red band of the electromagnetic spectrum and B8 stands for the infrared band (Fig. 3g).

2.2.7. Rainfall

Rainfall is an essential trigger for all three hazards in the study area, and the summer monsoon has caused landslides, debris flows and flash floods in the past few decades. A rainfall map was created based on the average monthly rainfall of 3-gauge stations located in the study region from 1981 to 2016 using the inverse distance weighted interpolation in ArcGIS 10.6 (Ullah and Zhang, 2020) (Fig. 3h).

2.2.8. Distance to roads

The distance to roads significantly impacts natural hazards in mountainous areas (Pourghasemi et al., 2019). Road construction alters the slope conditions in mountainous regions, which may affect debris flow and landslide susceptibility (Pourghasemi and Kerle, 2016; Pouyan et al., 2021). Distance to road was calculated from road network shapefile using Euclidean distance tool ArcGIS v.10.6 (Fig. 3i).

2.2.9. Stream power index (SPI)

SPI calculates the erosive power of groundwater based on an anticipated discharge, which causes toe erosion and river cutting (Wang et al., 2020a). SPI was calculated using Eq. (2).

$$\mathrm{SPI} = A_s \times \tan\beta \tag{2}$$

where A_s denotes the specific catchment area in meters and β denotes the slope in degrees (Fig. 3j).

2.2.10. The sediment transport index (STI)

STI is a method for calculating erosion and sedimentation rates (Rahman et al., 2021). This is one important factor in assessing flash floods, debris flow and landslide in areas where erosion and depositional processes are happening (Pham et al., 2020; Mandal et al., 2021; Rahman et al., 2021). In our study STI has no impacts on landslide so this factor was not used in landslide in our study, and is calculated by Eq. (3) (Fig. 3k).

$$\mathrm{STI} = \left(\frac{a}{22.13}\right)^{0.6}\left(\frac{\sin\beta}{0.0896}\right)^{1.3} \tag{3}$$

2.3. 11 Aspect

In the case of landslides and floods, the aspect has proven to be a critical element (Chen et al., 2020; Pham et al., 2020; Fang et al., 2021). Aspects influence hydrological processes (evaporation, weather, plant, and root development), as well as meteorological events such as rainfall, sunshine, and dry winds, that influence landslide, debris flow and flood events (Ullah and Zhang, 2020; Wang et al., 2020a) (Fig. 3l).

2.3.1. Topographic wetness index (TWI)

The TWI indicates the locations and sizes of water-saturated zones. This index is crucial for debris flow, landslides and floods since it can provide details about the humidity of various soil types (Khosravi et al., 2016; Ullah and Zhang, 2020). Consequently, the concentration of moisture in the soil affects both infiltration and runoff. The TWI was calculated using Eq. (4),

Table 2
Geological age and formation of the study area.

Abbreviation	Age	Unit name	Lithological units
CG	Cretaceous	Swat and Mansehra Granite Complexes Undivided	Granites and gneiss
ISM	Mesozoic	Indus Suture Melange	Mélange and marble green
KK	Cretaceous	Kamila amphibolite	Calc Alkaline metabasal
MM	Mesozoic	Kashala, Nikanai ghar and Saidu Formations Undivided	Schist, Marble and phyl
PCB	Precambrian	Besham and Kotla Complexes Undivided	Gneiss
PCQ	Precambrian	Tanawal Formation and Manglaur Formations Undivided	Quartzite and schists
PCS	Precambrian	Korara Complex and Gandaf Formations Undivided	phyllite, schist, barbl

$$TWI = \ln\left(\frac{\alpha}{\tan\beta}\right) \quad (4)$$

where α denotes the accumulation of flow around a point and β denotes the associated slope (Fig. 3m).

2.3.2. Landcover

Land cover directly or indirectly affects evapotranspiration, infiltration, runoff generation, and sediment dynamics, and significantly impacts the functions of hydrological and geomorphological dynamics (Chen et al., 2020; Ullah and Zhang, 2020; Azarafza et al., 2021). A landcover map of 2020 with 30-m resolution was downloaded from www.globallandcover.com (Fig. 3n).

It should be noted that avoiding the uncertainties associated with different spatial resolutions is very challenging (Fang et al., 2020). Therefore, to be consistent with other causative factor maps and improve processing and storage efficiency, all the factors have been resampled with a spatial resolution of 12.5 m (Mandal et al., 2021).

3. Methodology

3.1. Factor screening

3.1.1. Multicollinearity analysis

To check the correlations between the causative factors, the Pearson correlation coefficient (PCC) was used. PCC is a statistical linear correlation coefficient that is commonly used to determine the linear relationship between variables (Kalantar et al., 2019). The PCC between two sets of samples A_i (i = 1, 2, 3,. . ., n) and B_j (j = 1, 2, 3,. . ., n) can be represented as Eq. (5):

$$PCC = \frac{\sum_{i=1}^{n}(a_i - \bar{a})\sum_{i=1}^{n}(b_j - \bar{b})}{\sqrt{\sum_{i=1}^{n}(a_i - \bar{b})^2 \sum_{i=1}^{n}(b_j - \bar{b})^2}} \quad (5)$$

where a_i and b_j are variable values for A_i and B_j, $\bar{a}$ and $\bar{b}$ are the average of A_i and B_j, respectively. In general, the higher the absolute value of the PCC, the greater the risk of multicollinearity between variables (Jiang and Chen, 2016). The PCC value above 0.70 indicates multicollinearity, meaning that the input variables have a common contribution. In this case, the variable should be removed from the training procedure (Kalantar et al., 2020).

3.1.2. Mean decrease Gini

We used a random forest algorithm using the mean decrease Gini (MDG) to determine the importance of causative variables in the incidence of environmental hazards in the study area. This index is very reliable in assessing the significance of influential factors, particularly when environmental factors are associated (Nicodemus, 2011). The MDG is computed as the Gini impurities decreasing from a particular factor standardized by trees (Calle and Urrea, 2011; Pouyan et al., 2021).

3.2. Multi-hazard spatial prediction

The selection of the terrain mapping unit (TMU) for studies of hazard susceptibility is critical (Wang et al., 2019). Four different terrain mapping units are widely used in the literature, namely slope terrain unit (STU), geo-hydrological terrain unit (GHTU), census terrain unit (CTU), and grid cell terrain unit (GCTU) (Zêzere et al., 2017). Grid cells are often used to model natural hazards susceptibility mapping, and GCTUs divide the study area into squared areas and assigns a value to each causative factor. In this study, we used GCTU as a mapping unit, after defining TMU, all the causative factors were resampled to the same grid size of 12.5 m × 12.5 m.

Fig. 4 depicts the entire workflow of the proposed framework, including the following main steps: (i) Preparation of multi-hazard inventories and causative factors; (ii) standardization and multicollinearity assessment of multi-hazard causative factors; (iii) CNN model construction and development of multi-hazard susceptibility prediction maps; (iv) validation and comparison and (v) multi-hazard susceptibility map.

3.2.1. Convolutional Neural Network (CNN)

CNN is a well-known DL algorithm that can perform image processing (Wang et al., 2020b). It is basically a multi-layer feed-forward neural network capable of extracting useful information from relevant data (Wang et al., 2020a). The CNN architecture comprises of convolutional layers, pooling layers, and fully connected layers (Yamashita et al., 2018). The convolutional layer is made up of multiple convolution kernels that extract complex and relevant features from the input data (Canziani et al., 2016; Mallat, 2016). A nonlinear activation function usually follows each feature map. To embed nonlinearity into the system, the activation function of rectified linear unit (ReLU) is considered in the convolutional layer. The convolution process extracts a lot of information from the input layer and enables weight sharing (Wang et al., 2019).

The pooling layer is generally used after the convolutional layer, and the dimension of the feature map is reduced by the down-sampling algorithm, thereby avoiding over-fitting and reducing the computational costs. The fully connected layer functions as a classifier and has the same structure as the traditional fully connected network. They are usually used to generate the final combination of nonlinear features to predict the end of the network architecture. Based on these basic layers, various extended CNN architectures have been proposed and applied in many fields, such as VGG (Simonyan and Zisserman, 2014), Google Net (Szegedy et al., 2015), etc. Moreover, the CNN algorithm has been successfully used in several environmental hazard studies (Wang et al., 2019, 2020a; Zhang et al., 2019; Mandal et al., 2021).

To build a suitable CNN algorithm, one should be pay close attention to hyperparameter tuning (LeCun et al., 2015). In particular, hyperparameters such as the size of the convolution and pooling layers, activation and loss functions, optimizers and learning rates require special attention (Fang et al., 2020). The convolution and pooling functions are defined by the size of the convolution and pooling layers (Choi et al., 2017). The activation procedure fully controls the estimation of nonlinear operations (Audebert et al., 2019). The loss function in the model mainly serves to evaluate the degree of dispersion between the actual and predicted results (Chen et al., 2014; Ranjbar et al., 2018). The optimizer continuously updates the input variables (Wang et al., 2019). This study develops a one-dimensional CNN (1D-CNN) to predict multi-hazards (flash floods, landslides, and debris flow) and the architecture of the proposed 1D-CNN model was shown in Fig. 5.

3.2.2. Logistic regression

Logistic regression (LR) is a sophisticated statistical technique for assessing dependent and independent variables (Ghosh and Maiti., 2021). Using this model, the data does not necessarily be normal and the variables can be either categorical or continuous (Goyes-Peñafiel and Hernandez-Rojas., 2021). In this technique, individual susceptibility maps were constructed considering a dependent variable (e.g., flash floods, landslides, and debris flows) with 1 indicating hazard locations and 0 indicating non-hazard locations. Positive and negative coefficients of the LR indicate their influence on multi-hazards and their role in their formation (Ghosh and Maiti, 2021; Goyes-Peñafiel and Hernandez-Rojas, 2021). Pre-

cisely, a positive coefficient implies that the variable is present in the area and enhances the likelihood of standalone hazard, whereas a negative coefficient shows that hazard is adversely associated to that variable. In the model-building process, the sig (p) value of the causative factors is <0.05, indicating they are statistically significant, whilst the value >0.05 indicates statistically insignificant (Ghosh and Maiti, 2021). The LR approach is mathematically expressed as Eqs. (6)–(8) (Ahmad et al., 2021).

$$p = \ln\left(\frac{p}{1-p}\right) \tag{6}$$

$$p = \frac{1}{1+e^{-Z}} \tag{7}$$

$$Z = I_0 + I_1 \times C_1 + I_2 \times C_2 + I_3 \times C_3 + \cdots + I_n \times C_n \tag{8}$$

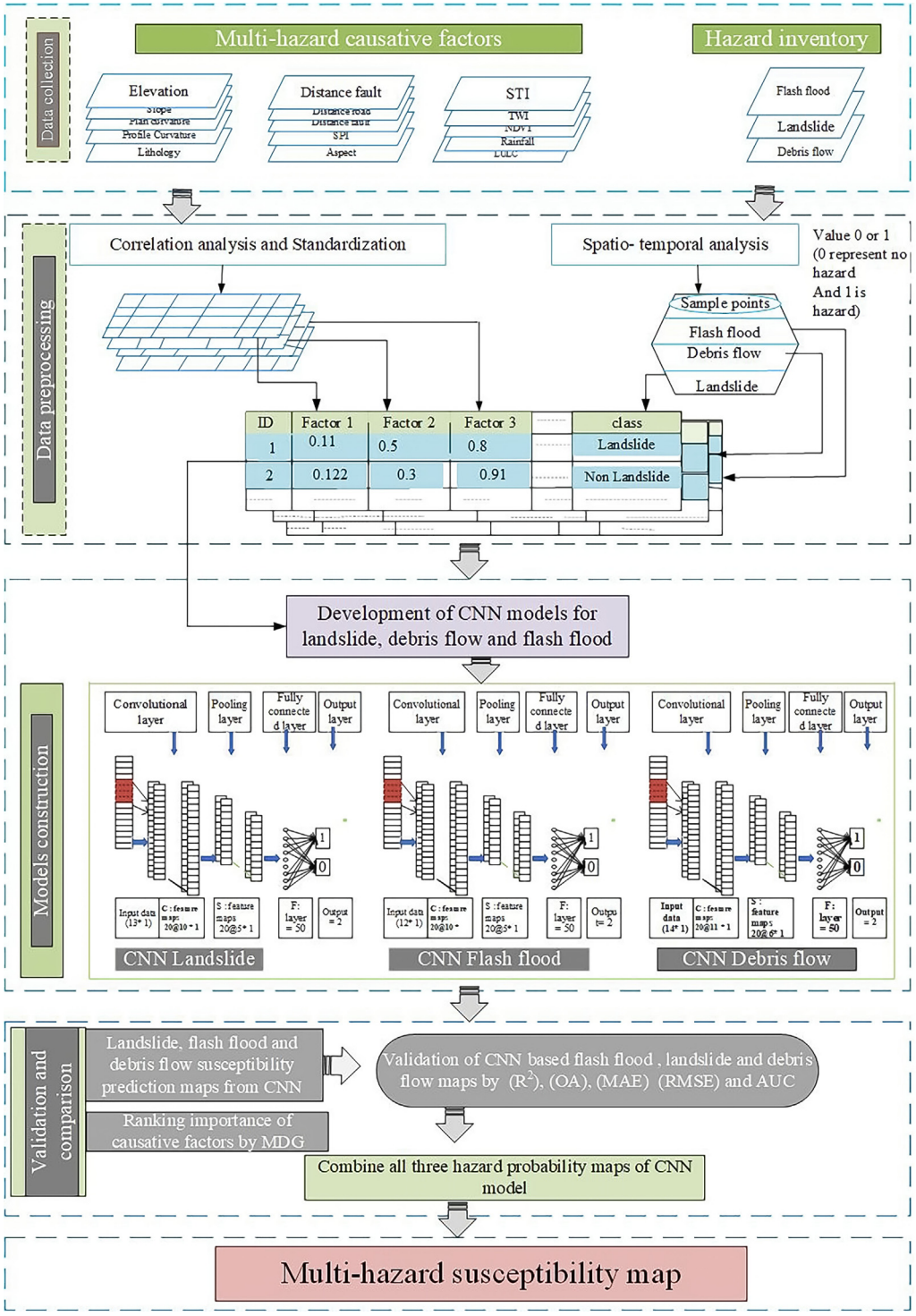

Fig. 4. Schematic flowchart of the study.

where p is the probability of the presence of the standalone hazard or non-hazard, Z is the linear combination, n represents the conditioning factors, C_i (i = 0, 1, 2,. . ., n) are the conditioning factors, I_0 is the intercept of LR model, and I_i (i = 0,1,2,. . ., n) are the LR coefficients for the independent variables.

3.2.3. K-nearest neighbor

K-nearest neighbor (KNN) has been widely used as a benchmark classifier in the field of artificial intelligence (AI) for quite some time now (Sun et al., 2022). The KNN is a simple nonparametric method for classifying (Avand et al., 2019). KNN categorizes data by comparing a given test set with a set of training data that is similar to it (Avand et al., 2019). The simplicity of the nearest-neighbor classification system is one of its main advantages. Choosing the number of neighbors, k, and the distance metric to be used are the only two options available to the user. Further details on the KNN algorithm can be found in Abraham et al. (2021) and Hou et al. (2021).

3.3. Evaluation of model performance

Model performance is evaluated to determine the multi-hazard model's precision and predictive abilities. We compute the Area under the curve (AUC) based on receiver operating characteristic (ROC) curves that have been widely used in several classification tasks (Fang et al., 2020). In addition, the models are further examined by other statistical metrics, i.e., OA, R^2, MAE, and RMSE by Eqs. (9)–(12) (Fang et al., 2020; Rahman et al., 2021),

$$OA = \frac{TP + TN}{TP + FP + TN + FN} \tag{9}$$

where TP, FP, TN and FN mean true positive, false positive, true negative and false negative, respectively.

$$R^2 = 1 - \frac{\sum_{i=1}^{N}(P - A)^2}{\sum_{i=1}^{N}\left(A - \bar{A}\right)^2} \tag{10}$$

$$MAE = \frac{1}{N}\sum_{i=1}^{N}|(P - A)| \tag{11}$$

$$RMSE = \sqrt{\frac{\sum_{i=1}^{N}(P - A)^2}{\sum_{i=1}^{N}\left(A - \bar{A}\right)^2}} \tag{12}$$

where N represents the number of observations, P, A and $\bar{A}$ represent the predicted value, the actual value and the mean of the actual value, respectively.

3.4. Multi-hazard probability mapping

The CNN-based flash flood, landslide and debris flow hazard maps are combined to construct a multi-hazard map (MHM), which is grouped into four categories using the jeans natural break classification method: low, moderate, high and very high. According to a review of the literature, susceptibility classes of low and moderate were considered low hazard (0) conditions, while susceptibility classes of high and very high were considered high hazard (1) conditions (Pourghasemi et al., 2020; Yousefi et al., 2020; Rahman et al., 2021). To make the integration easier, we reassign the four class maps created for each hazard to two classes: 0 and 1. Class zero is low to moderate, and 1 represents high to very high susceptibility. Lastly, using ArcGIS (v. 10.6), all three hazards (flash flood (FF), landslide (LS) and debris flow (DF)) were combined using the Eq. (13),

$$MHM = FF + LS + DF \tag{13}$$

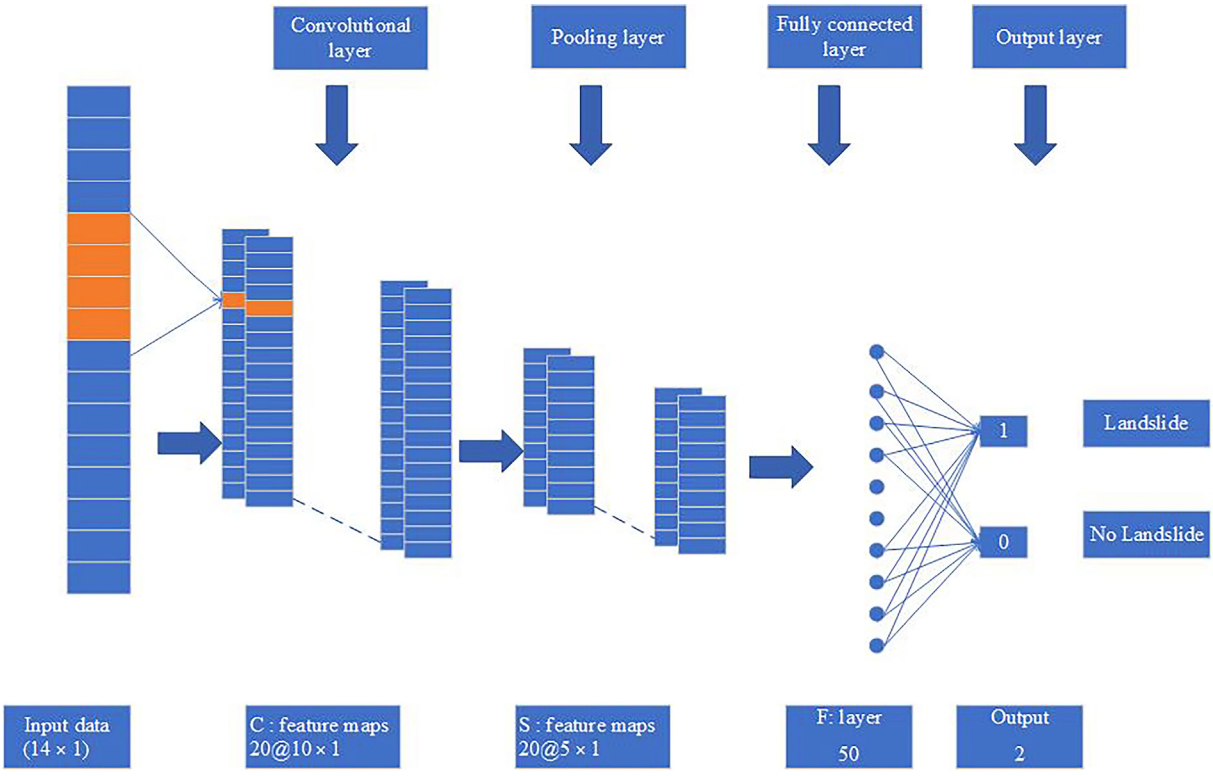

Fig.5. Landslide susceptibility mapping using the CNN architecture.

Based on the likelihood of multi-hazard occurrence, the final multi-hazard susceptibility map is classified into eight categories: no hazard, flash floods, landslides, debris flows, flash floods and debris flows, flash floods and landslides, landslides and debris flows, and all hazards.

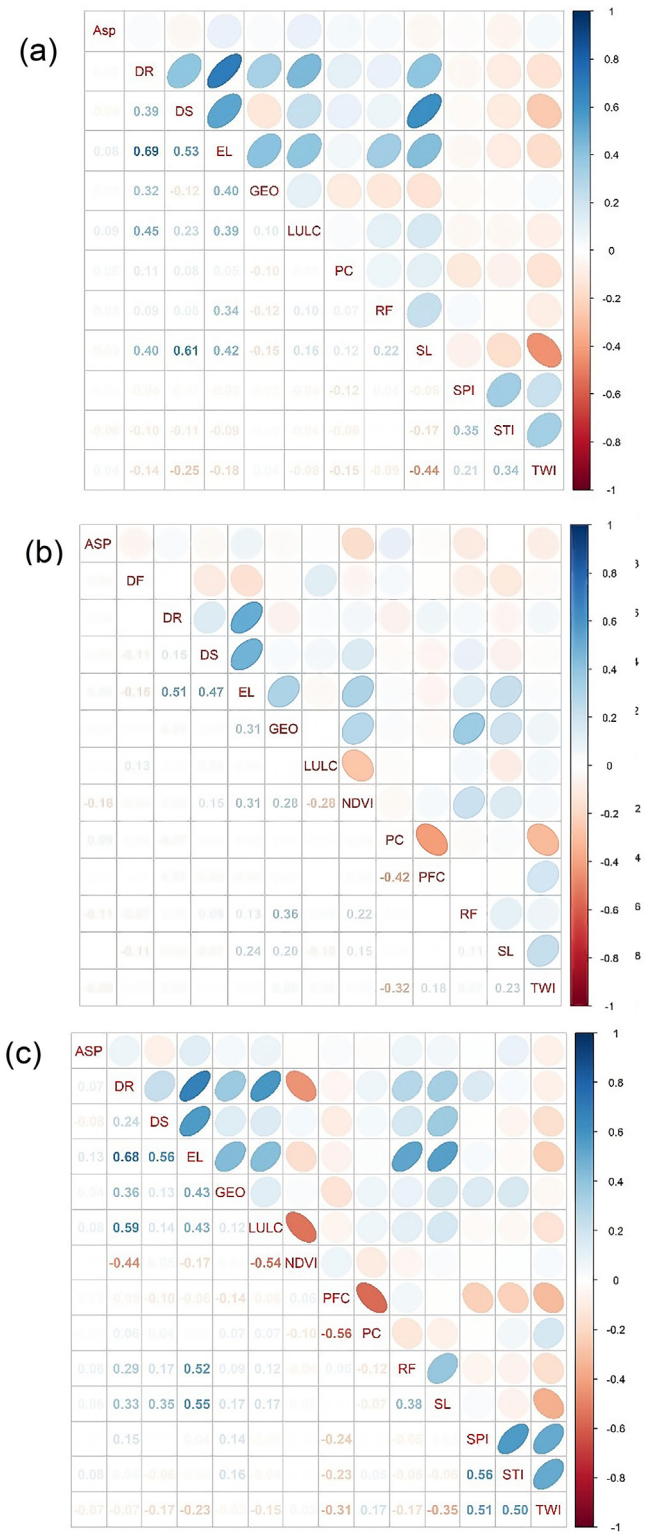

Fig. 6. Pearson correlation coefficients among multi-hazard causative factors: (a) flash flood, (b) landslide and (c) debris flow. ASP: aspect, DR: distance to road, DS: distance to stream, EL: elevation, GEO: geology, LULC: land cover, NDVI: normalized difference vegetation index, PFC: profile curvature, PC: plan curvature, RF: rainfall, SL: slope, SPI: stream power index, STI: sediment transport index, TWI: topographic wetness index, DF: distance to fault.

3.5. Contributions of causative factors

Fig. 6 shows the multicollinearity results of different causative factors in flash flood, landslide and debris flow hazards. According to the Pearson correlation coefficients (PCC) (<0.70), there was no multicollinearity in the selected causative factors for multi-hazard (flash flood, landslide and debris flow).

We used the random forest model to assess the significance of causative factors of multi-hazards (flash flood, debris flow and landslide). The results demonstrate that the factors of the slope, elevation, rainfall, distance to road, distance to stream, and TWI were the most important factors for predicting debris flow, as shown in Fig. 7a. For landslide hazard, MDG shows that slope, TWI, rainfall, elevation, distance to fault, and plan curvature were the most influential factors in predicting landslides, as shown in Fig. 7b. Finally, the most critical causative factors in flash flood hazard were slope, distance to stream, TWI, distance to roads, SPI, and elevation, as shown in Fig. 7c.

3.6. Single hazard maps

In this subsection, Convolutional Neural Network (CNN) was used to produce flash flood, landslide, and debris flow hazard susceptibility maps individually, as shown in Fig. 8. To construct the CNNs, all the hyperparameters were optimized using the trial-and-error process for flash floods, landslides, and debris flow, as demonstrated in Table 3. For the spatial pattern of risk estimation, it is important to classify the risk indices of landslides, flash floods, and debris flows into different categories (Tehrany et al., 2015). In this study, the Jenk's natural break method (Ullah and Zhang, 2020; Wang et al., 2020a,b) was used to classify the risk levels into low, moderate, high, and very high. In the case of landslide hazard, it can be easily observed from Figs. 8a and 9a that approximately 5.32%, 13.16%, 14.56%, and 36.97% of the study area had low, moderate, high, and very high susceptibility, respectively. Flash flood hazard map shows that about 35.32%, 13.16%, 14.56%, and 36.97% of the study area had low, moderate, high, and very high susceptibility, respectively (Figs. 8b and 9a). In debris flow hazard, approximately 46.77%, 18.11%, 13.97%, and 21.15% of the study area had low, moderate, high, and very high susceptibility, respectively (Figs. 8c and 9a).

3.7. Multi-hazard susceptibility mapping

To generate a multi-hazard susceptibility map, all three susceptibility maps of selected hazards generated by CNN were combined using Eq. (13), as shown in Fig. 10. We can observe from Fig. 9b that 37.64% of the study area was safe and had not suffered any hazard. In contrast, 16.18 % of the total area was vulnerable to flash flood hazards, 4.88% of the area was vulnerable to debris flow hazards and 30.68% of the total area was vulnerable to landslide hazards in the study area, as shown in Fig. 9b. Meanwhile, 0.27%, 7.05%, and 3.13% of the study area were susceptible to at least two types of hazards: flash floods and debris flows, debris flows and landslides, and flash floods and landslides, respectively (Figs. 9b and 10). Finally, a total of 0.17% of the study area were determined to be prone to all hazards, i.e., landslides, flash floods, and debris flows (Figs. 9b and 10).

3.8. Validation and comparison

To check the accuracy of our CNN models, we used several statistical indices and compared CNN models with conventional mod-

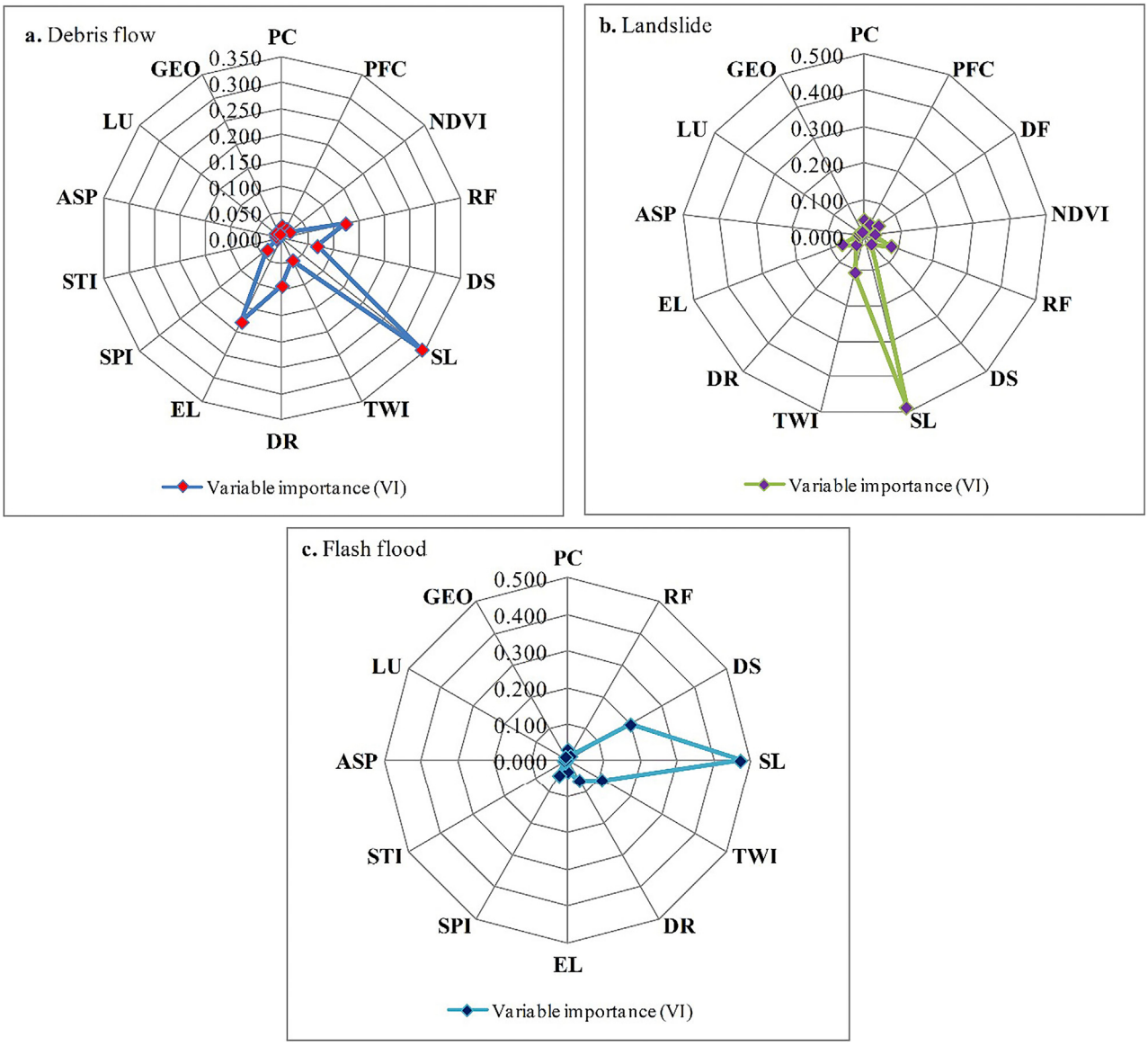

Fig.7. Multi-hazard variable importance by RF: (a) debris flow, (b) landslide and (c) flash flood.

els LR and KNN, as shown in Table 4. The CNN model outperformed the conventional LR and KNN in predicting all three hazards. The CNN model used for predicting flash floods has the highest overall accuracy of 96%, followed by LR and KNN with 94% and 84%, respectively. Also, the CNN model used for predicting debris flows has the highest overall accuracy of 94%, followed by LR and KNN with 90% and 87%, respectively. The CNN and LR models used for predicting landslides have the same overall accuracy of 90%, which is 10% higher than that of KNN.

Similarly, we notice that similar trends in all other evaluation indices and the CNN model can demonstrate the best performance in susceptibility prediction, followed by LR and KNN. Fig. 11 depicts the ROC curves of the three models. In all three hazards, CNN is superior to the conventional machine learning models of LR and KNN. Specifically, CNN achieved the highest AUC value for flash floods (0.98) (Fig. 11a), landslides (0.94) (Fig. 11b), and debris flows (0.98) (Fig. 11c).

4. Discussion

Over the past few years, multi-hazard assessments of environmental hazards have become increasingly important, underscoring the need for a more comprehensive framework (Pourghasemi and Kerle, 2016; Sanam et al., 2020). Despite the increased interest in multi-hazard susceptibility modeling, independent assessments are still conducted by communities concerned with the topic. To achieve this, various methods have been used to analyze multi-hazards globally (Javidan et al., 2021). Specifically, we propose a method that makes it easier to identify areas that are simultaneously threatened by multiple hazards (e.g., flash floods, landslides, and debris flows) in the context of this study. We achieve this goal by combining deep learning with GIS.

Initially, the multi-collinearity of multi-hazard causative factors was assessed through PCC. In addition, a random forest algorithm was used considering the MDG method to determine the impor-

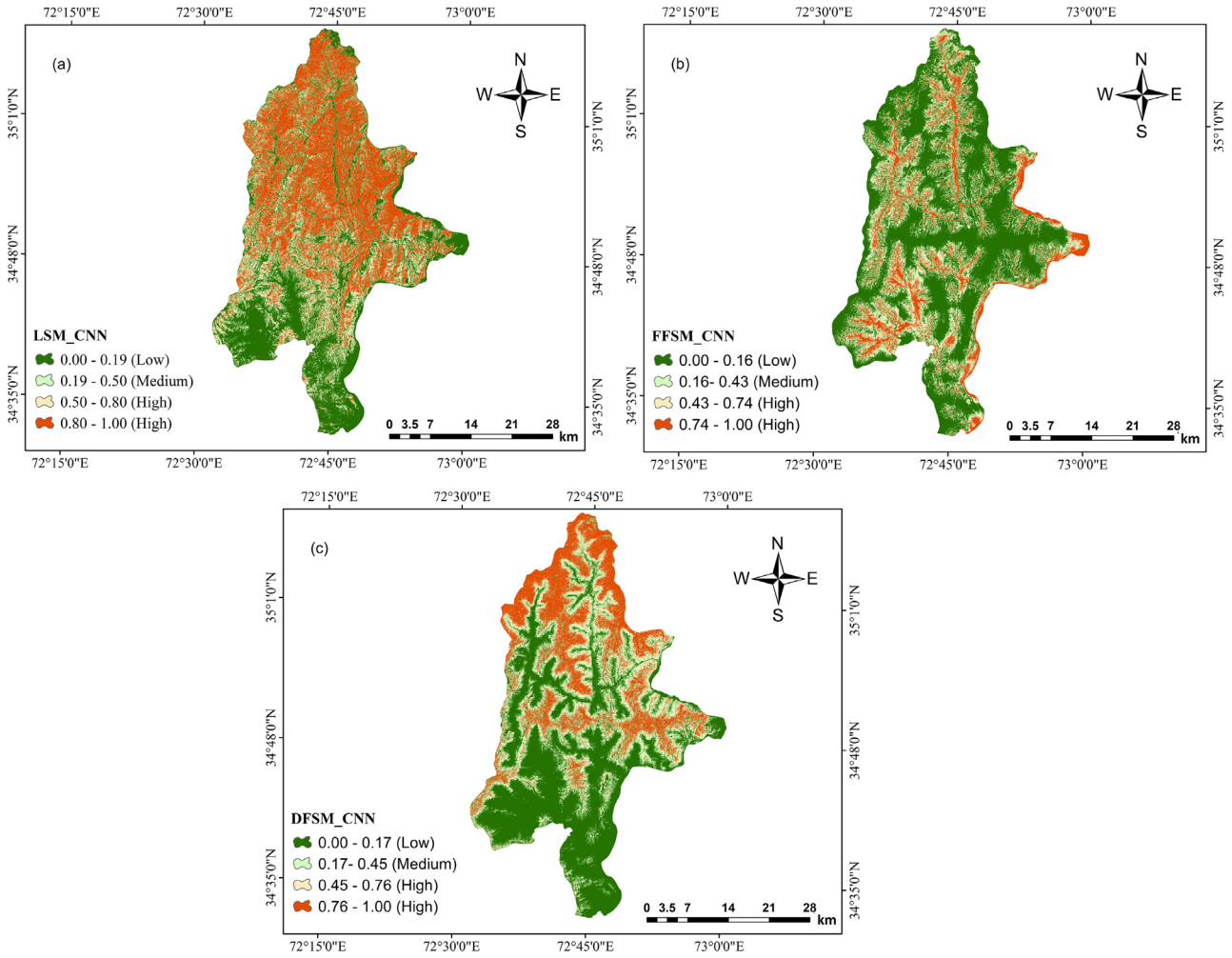

Fig. 8. Single hazard susceptibility maps. (a) LSM_CNN: landslide susceptibility map by CNN, (b) FFSM_CNN: flash flood susceptibility map by CNN and (c) DFSM_CNN: debris flow susceptibility map by CNN.

Table 3
Hypermeters settings of the CNN models.

CNNs	Parameters						
	Convolutional kernel size	Max pooling kernel size	Number of epochs	Activation function	Loss function	optimizer	Learning rate
CNN LSM	3 × 1	2 × 1	200	ReLu	Categorical cross entropy	AdaGrad	0.01
CNN FFSM	3 × 1	2 × 1	150	ReLu	Categorical cross entropy	AdaGrad	0.05
CNN DFSM	3 × 1	2 × 1	50	ReLu	Categorical cross entropy	AdaGrad	0.009

tance of the hazard-related causative factors. As shown in Fig. 6, there is no multicollinearity in the causative factors of flash floods, landslides, and debris flow. Meanwhile, the MDG results demonstrate that slope angle, distance to stream, and TWI were the most important factors in predicting flash floods, as shown in Fig. 7. Previous studies (Pourghasemi et al., 2020; Wang et al., 2020a) can support these observations because flooding is more likely to occur in flat areas, with greater accumulation of discharge and less runoff (Ullah and Zhang, 2020; Rahman et al., 2021). The heavy downpours significantly increased the flow and sediment deposition in the areas near the river basin and increased the possibility of flooding in these areas (Pourghasemi et al., 2019; Yousefi et al., 2020). In addition, TWI measures flow accumulation and a higher TWI value means a higher risk of flooding (Khosravi et al., 2016; Das, 2019; Costache et al., 2020). The areas most prone to flooding are close to rivers, with lower elevations and less slopes, and are usually used for agricultural or residential purposes (Khosravi et al., 2019). As for landslides, the most important factors were slope, elevation, rainfall, and distance to roads. The occurrence of landslides increases as the elevation and the slope are increased (Pourghasemi et al., 2019). Rainfall is also the main landslide triggering factor and sudden and intense rainfall or snowmelt can cause movement (Wang et al., 2019). TWI measures the dryness and wetting of soil moisture, which is a main cause of landslides (Fang et al., 2020). The most important factors affecting debris flow risk were slope, elevation, rainfall, and distance to roads. Kritikos

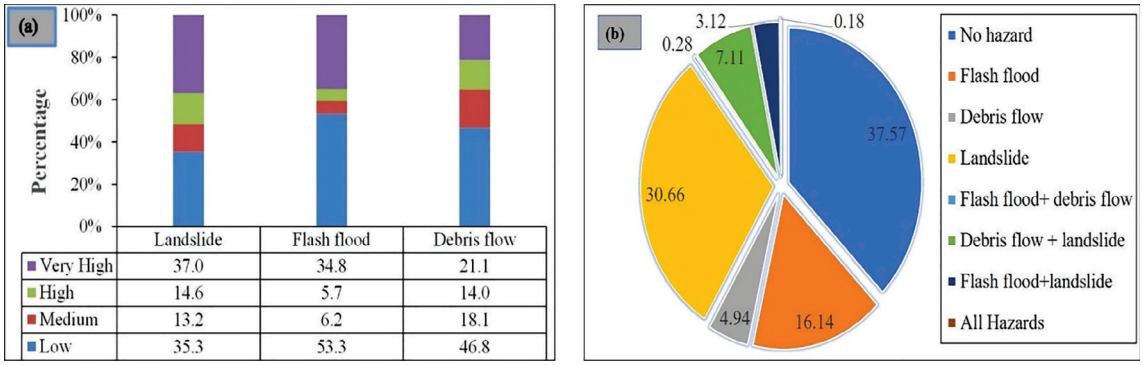

Fig. 9. (a) Individual hazard distribution based on CNN and (b) proportion of the study area vulnerable to single and multi-hazard.

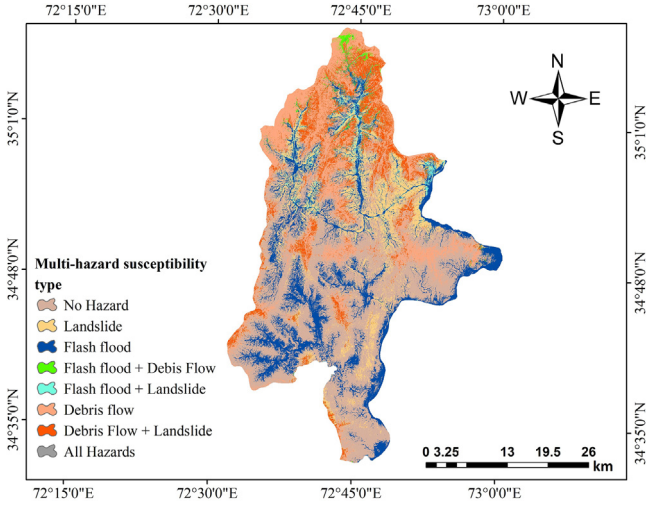

Fig. 10. Multi-hazard susceptibility map.

and Davies (Kritikos et al., 2015) pointed out in 2015 that on steep slopes, the downslope factor of gravity is greater, resulting in an increase in the shear stress of the slope and makes the surface material of the slope more susceptible to damage, and provides a favorable environment for the occurrence of debris flow. Rainfall is also an important trigger of debris flow. Debris flows are usually associated with heavy precipitation or snowmelt periods and will exacerbate the flooding effects that often accompany such events (Marra et al., 2017; Wu et al., 2019). More precisely, according to Chousianitis et al. (2016), the effects of earthquakes and rainfall on slope stability vary by season. Precipitation may increase the risk of landslides in summer season as soils become saturated, thereby reducing slope stability. Also, flooding is more likely when natural or man-made drainage systems are overwhelmed by prolonged or heavy rainfall.

Understanding the interrelationships between different hazards is a significant challenge (Kappes et al., 2010). To the best of our knowledge, there is no research on using CNN, a deep learning model to carry out multi-hazard susceptibility mapping in the present test site. The practicality of CNN was validated in this study for multi-hazard susceptibility prediction compared to conventional LR and KNN models. Several accuracy indices were used to evaluate CNN multi-hazard models (flash floods, landslides, debris flow) effectiveness and predictive capacity. The experimental results demonstrate that CNN revealed the highest accuracy in mapping the susceptibility of flash floods, landslides, and debris flows at the test site (Table 4). CNN model was superior to the conventional machine learning LR and KNN models in predicting flash floods, debris flows, and landslides. The CNN model is considered an excellent natural hazard modeling tool around the world (Chen et al., 2014; Wang et al., 2019, 2020a; Zhang et al., 2019; Bui et al., 2020) due to its excellent results and higher prediction accuracy for spatial prediction of natural hazards. Machine learning methods such as LR and KNN still cannot be ignored, though CNN provides an accurate spatial prediction of flash floods, landslides, and debris flows. It is known that CNN and machine learning methods have achieved high accuracy in remote sensing, geoscience, and natural hazards research on a global scale (Avand et al., 2019; Roy and Saha, 2019; Wang et al., 2019). However, special consideration must be given to the interpretation of their results. The performance of a CNN model is governed by its architecture, including the structure of training data, the amount of the input data, activation function, and convolutional and pooling layers (Wang et al., 2019; Zhao et al., 2020). Using trial and error to optimize the parameters of CNN, it is possible to improve the accuracy of the algorithm.

Table 4
Validation of model results using different statistical measures.

Disaster type	Model	Validation using test data set				
		R^2	MAE	RMSE	OA	AUC
Flash Flood	CNN	**0.85**	**0.05**	**0.19**	**0.96**	**0.98**
	LR	0.83	0.1	0.21	0.94	0.97
	KNN	0.69	0.2	0.28	0.84	0.95
Landslide	CNN	**0.65**	**0.15**	**0.3**	**0.9**	**0.94**
	LR	0.6	0.23	0.32	0.9	0.94
	KNN	0.38	0.32	0.39	0.8	0.86
Debris flow	CNN	**0.78**	**0.11**	**0.23**	**0.94**	**0.98**
	LR	0.63	0.19	0.3	0.9	0.93
	KNN	0.61	0.23	0.31	0.87	0.95

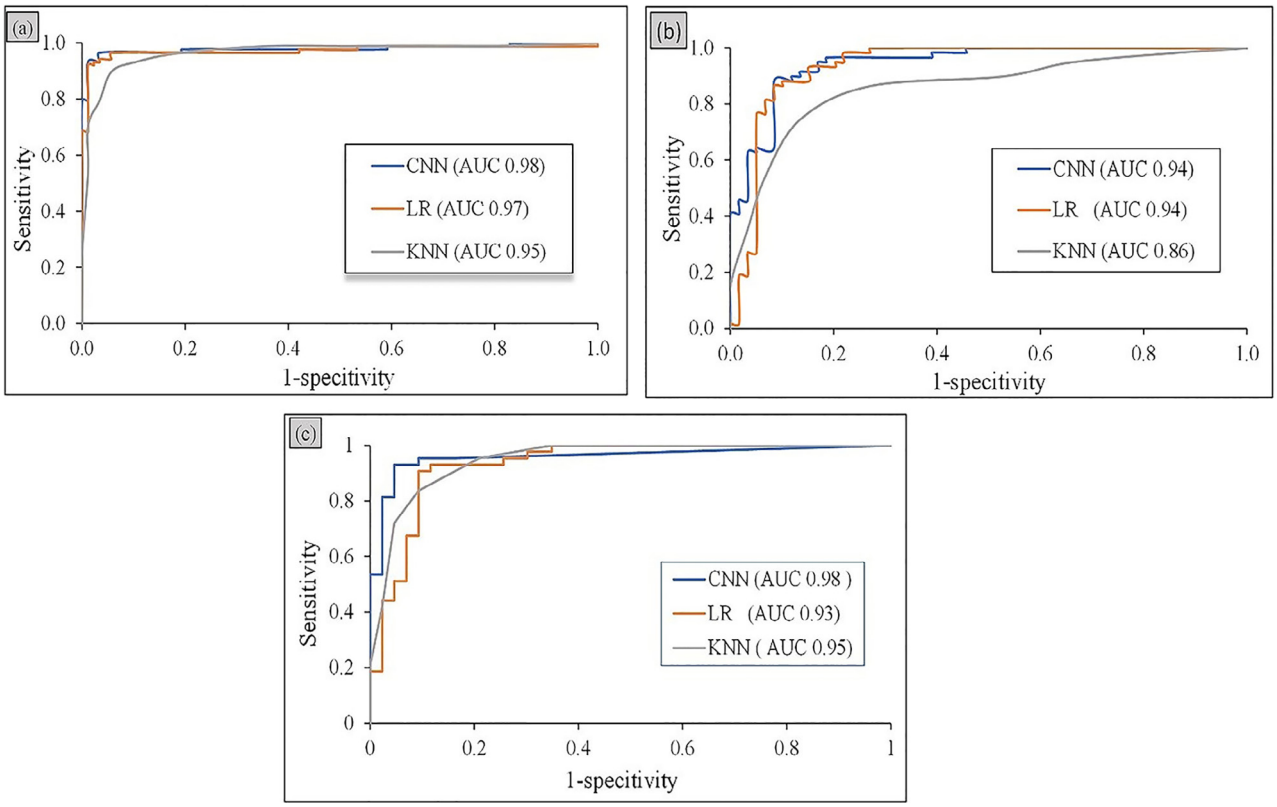

Fig. 11. ROC curve for (a) flash flood, (b) landslide and (c) debris flow by CNN, LR and KNN, respectively.

Recently, Wang et al. (2019, 2020a) used different CNN structures of 1D-CNN, 2D-CNN and 3D-CNN to perform landslide and flood susceptibility and compared the results with machine learning methods. The results confirmed that CNN is better than conventional machine learning models. They also proposed that integrating CNN with other conventional machine learning classifiers can improve prediction results than the CNN model alone. Mandal et al. (2021) conducted a study on landslide susceptibility in India and stated that performance of CNN is more effective than machine learning methods (such as ANN, RF and bagging). Pham et al., (2020) used CNN and RF Random subspace to generate a landslide susceptibility map in the mountainous region of Vietnam, and CNN demonstrated a prediction accuracy of 0.88%. In this study, CNN has achieved a prediction accuracy of 0.98%, 0.97%, and 0.94% using the validation data sets of flash floods, landslides and debris flow, respectively (Table 4), indicating that the highly accurate multi-hazard susceptibility map of district Shangla, eastern Hindu Kush Pakistan can be obtained. Our results are consistent with previous studies that CNN performs better prediction in environmental hazard susceptibility prediction (Pham et al., 2020; Mandal et al., 2021).

The CNN prediction maps for flash floods, landslides and debris flows were combined to produce a multi-hazard susceptibility map shown in Fig. 9. The multi-hazard susceptibility map shows that about 37.57% of the study area is not vulnerable to any hazard. The remaining 62.43% of the study area is susceptible to one or more hazards of which 0.18% of the total area was exposed to all three hazards, as shown in Fig. 10b.

Most studies are inconsistent in spatial resolution of multi-hazard dependent variables (Catani et al., 2013; Costache et al., 2019; Rahman et al., 2021), which is the main limitation of the present study. To avoid the uncertainties associated with different spatial resolutions and to improve processing and storage efficiency, all factors have been resampled (Fang et al., 2020). DL with high-resolution environmental factors may extract more sophisticated information about the hazard and its surroundings (Ma et al., 2019), which could be very useful in understanding the multi-hazard situation. However, high spatial resolution factors like DEM and its derivatives may not improve the performance of natural hazard susceptibility mapping, and finding the optimal resolution needs a series of experiments (Merghadi et al., 2020). The second limitation of this study is that we only selected landslide, debris flow, and flash flood hazards in the study area based on data availability and disaster information. Other hazards like glacier avalanches and forest fires are also present in the study area. A comprehensive multi-hazard susceptibility should account for each hazard present in the study area, but a lack of data restricts us to the subset of hazards.

Furthermore, we only selected static causative factors for multi-hazard susceptibility prediction and they perform well in describing historical hazards in the region but unplanned urbanization and climate change significantly changing the environment in Hindu Kush Pakistan which may reshape the distribution of future hazards (Eckstein et al., 2021). Especially, Pakistan is one of the most affected countries affected by climate change (Eckstein et al., 2021) and it is expected to increase the appearance of multiple hazards in mountain areas of Hindukush Pakistan (Allan et al., 2021; Eckstein et al., 2021). As a result, future studies will focus on the potential impact of climate and land use/land cover change on multi-hazard using different deep learning models like CNN 2D, CNN 3D, RNN and DNN etc.

Despite the limitations, our study presented a robust framework for multi-hazard susceptibility prediction in complex topographic and climatic regions of eastern Hindukush, district Shangla, Pakistan. We believe our findings will help in multi-hazard risk management. Specifically, authorities can use our

multi-hazard susceptibility map by the CNN model to identify and rank susceptible areas.

Finally, the proposed method is also applicable to other environmental hazards, such as glacier avalanches, land subsidence, and forest fire susceptibility. Based on the observations, policymakers can develop effective interventions to mitigate the impact of multi-hazards on people, particularly those living in disasters.

Even though individual hazard susceptibility maps are important, multi-hazard susceptibility maps allow for spatial and quantitative analysis of commodified information occurring within a site (Pourghasemi et al., 2019). Indeed, it offers authorities and policymakers estimates of where to focus and respond after disasters, allowing them to gain a more complete perspective of how multi-hazards are likely to occur (Marin et al., 2021). Besides, the obtained multi-hazard map can help emergency response agencies conduct their operations more efficiently in the pre-disaster and post- disaster phases. We should emphasize the relevance of hazard communication with stakeholders outside academia (Graham et al., 2022). Geoscientists, hydrologists, and related researchers may be able to conclude that multi-hazard maps are more complex. However, they can be challenging for policymakers, emergency personnel, and others who make decisions to comprehend information (Rahman et al., 2021). To effectively convey multi-hazard information to non-experts, maps should be constructed as simply as possible to avoid misunderstanding and help individuals quickly identify the locations of different levels of potential hazards provided on the map (Javidan et al., 2021). This can be done by providing accompanying documents that provide a brief description of the processes that may lead to the appearance of things considered vulnerable, as well as pictures and videos of the damage caused by these things, so that people can get a general idea about what they can do (Graham et al.,2022). We therefore stress the importance of multi-hazard psychology (e.g., using photographs of past disasters), information presentation (e.g., accessible to non-technical and non-experts), and appropriate presentation schemes for multi-hazard countermeasures (Karpouza et al., 2021).

5. Conclusions

Flash floods, debris flows, and landslides frequently occurred in the Hindukush area, which is vulnerable to multiple hazards. Therefore, a comprehensive method is needed to consider multiple hazards and their individual and combined causative factors. In this regard, this study aims to present a deep learning framework to predict the susceptibility of multi-hazard in the Shangla district, eastern Hindukush, Pakistan. The resultant multi-hazard map shows that approximately 37.57% of the study area can avoid the possibility of all the three hazards, while about 62.43% of the study area is prone to multi-hazards (one or more hazards). Nevertheless, the proposed algorithm is feasible and applicable in mapping multi-hazards. The CNN-based algorithm can improve the ability to predict the risk of multi-hazards and increase the awareness of multiple disasters. Local authorities can use the multi-hazard maps constructed in this study to establish multi-hazard mitigation and emergency evacuation management plans, and serve as insurance requirements for any property. In addition, it can be applied to similar geo-environments, especially in mountainous areas with sparse data.

Declaration of Competing Interest

The authors declare that they have no known competing financial interests or personal relationships that could have appeared to influence the work reported in this paper.

Acknowledgements

This work was supported by the Joint Funds of the National Natural Science Foundation of China (U21A2013), the State Key Laboratory of Biogeology and Environmental Geology, China University of Geosciences (GBL12107) and the National Natural Science Foundation of China (61271408). The authors would like to thank Latif and Sardar Wajid for helping in field visit and data collection (landslide and debris flow points). The authors would also like to thank the Associate Editor Prof. Biswajeet Pradhan, and three anonymous reviewers for their constructive comments, which improved the manuscript.

References

Abedi Gheshlaghi, H., Feizizadeh, B., Blaschke, T., Lakes, T., Tajbar, S., 2021. Forest fire susceptibility modeling using hybrid approaches. Trans GIS 25, 311–333.
Abraham, M.T., Satyam, R., Pradhan, B., et al., 2021. Factors Affecting Landslide Susceptibility Mapping: Assessing the Influence of Different Machine Learning Approaches, Sampling Strategies and Data Splitting. Land 10 (9). https://doi.org/10.3390/land10090989. In press.
Abuzied, S.M., Pradhan, B., 2021. Hydro-geomorphic assessment of erosion intensity and sediment yield initiated debris-flow hazards at Wadi Dahab Watershed, Egypt. Georisk Assess. Manag. Risk Eng. Syst. Geohazards 15, 221–246.
Ahmad, H., Ningsheng, C., Rahman, M., Islam, M.M., Pourghasemi, H.R., Hussain, S.F., Habumugisha, J.M., Liu, E., Zheng, H., Ni, H., Dewan, A., 2021. Geohazards susceptibility assessment along the upper indus basin using four machine learning and statistical models. ISPRS Int. J. Geoinf. 10, 315.
Aksha, S.K., Resler, L.M., Juran, L., Carstensen Jr, L.W., 2020. A geospatial analysis of multi-hazard risk in Dharan, Nepal. Geomatics, Nat. Hazards Risk 11, 88–111.
Ali, S., Haider, R., Abbas, W., Basharat, M., Reicherter, K., 2021. Empirical assessment of rockfall and debris flow risk along the Karakoram Highway, Pakistan. Nat. Hazards 106, 2437–2460.
Allan, R.P., Hawkins, E., Bellouin, N., Collins, B., 2021. IPCC, 2021: Summary for Policymakers.
Atta-Ur-Rahman, Shaw, Rajib, 2015. Flood Risk and Reduction Approaches in Pakistan. Disaster Risk Reduction Approaches in Pakistan. Springer Nature, pp. 77–100.
Audebert, N., Le Saux, B., Lefèvre, S., 2019. Deep learning for classification of hyperspectral data: A comparative review. IEEE Geosci. Remote Sens. Mag. 7, 159–173.
Avand, M., Janizadeh, S., Naghibi, S.A., Pourghasemi, H.R., Khosrobeigi Bozchaloei, S., Blaschke, T., 2019. A comparative assessment of random forest and k-nearest neighbor classifiers for gully erosion susceptibility mapping. Water 11, 2076.
Azarafza, M., Azarafza, M., Akgün, H., Atkinson, P.M., Derakhshani, R., 2021. Deep learning-based landslide susceptibility mapping. Sci. Rep. 11, 1–16.
Azareh, A., Rafiei Sardooi, E., Choubin, B., Barkhori, S., Shahdadi, A., Adamowski, J., Shamshirband, S., 2021. Incorporating multi-criteria decision-making and fuzzy-value functions for flood susceptibility assessment. Geocarto Int 36, 2345–2365.
Bathrellos, G.D., Skilodimou, H.D., Chousianitis, K., Youssef, A.M., Pradhan, B., 2017. Suitability estimation for urban development using multi-hazard assessment map. Sci. Total Environ. 575, 119–134.
Bronkhorst, V.B., 2012. Disaster Risk Management in South Asia: Regional Overview. The World Bank.
Bui, D.T., Hoang, N.-D., Martínez-Álvarez, F., Ngo, P.-T.-T., Hoa, P.V., Pham, T.D., Samui, P., Costache, R., 2020. A novel deep learning neural network approach for predicting flash flood susceptibility: A case study at a high frequency tropical storm area. Sci. Total Environ. 701, 134413.
Calle, M.L., Urrea, V., 2011. Letter to the editor: stability of random forest importance measures. Brief. Bioinform. 12, 86–89.
Canziani, A., Paszke, A., Culurciello, E., 2016. An analysis of deep neural network models for practical applications. arXiv Prepr. arXiv1605.07678.
Cao, J., Zhang, Z., Du, J., Zhang, L., Song, Y., Sun, G., 2020. Multi-geohazards susceptibility mapping based on machine learning—a case study in Jiuzhaigou, China. Nat. Hazards 102, 851–871.
Catani, F., Lagomarsino, D., Segoni, S., Tofani, V., 2013. Landslide susceptibility estimation by random forests technique: sensitivity and scaling issues. Nat. Hazards Earth Syst. Sci. 13, 2815–2831.
Chen, J., Li, Y., Zhou, W., Iqbal, J., Cui, Z., 2017. Debris-flow susceptibility assessment model and its application in semiarid mountainous areas of the Southeastern Tibetan Plateau. Nat Hazards Rev. 1, 05016005.
Chen, Y., Lin, Z., Zhao, X., Wang, G., Gu, Y., 2014. Deep learning-based classification of hyperspectral data. IEEE J. Sel. Top. Appl. Earth Obs. Remote Sens. 7, 2094–2107.
Chen, Y., Qin, S., Qiao, S., Dou, Q., Che, W., Su, G., Yao, J., Nnanwuba, U.E., 2020. Spatial Predictions of Debris Flow Susceptibility Mapping Using Convolutional Neural Networks in Jilin Province, China. Water 12, 2079.
Choi, K., Fazekas, G., Sandler, M., Cho, K., 2017. Convolutional recurrent neural networks for music classification. In: 2017 IEEE International Conference on Acoustics, Speech and Signal Processing (ICASSP). IEEE, pp. 2392–2396.

Choubin, B., Borji, M., Mosavi, A., Sajedi-Hosseini, F., Singh, V.P., Shamshirband, S., 2019. Snow avalanche hazard prediction using machine learning methods. J. Hydrol. 577, 123929.
Costache, R., Hong, H., Wang, Y., 2019. Identification of torrential valleys using GIS and a novel hybrid integration of artificial intelligence, machine learning and bivariate statistics. Catena 183, 104179.
Costache, R., Popa, M.C., Bui, D.T., Diaconu, D.C., Ciubotaru, N., Minea, G., Pham, Q.B., 2020. Costache, R., Popa, M.C., Bui, D.T., Diaconu, D.C., Ciubotaru, N., Minea, G. and Pham, Q.B., 2020. Spatial predicting of flood potential areas using novel hybridizations of fuzzy decision-making, bivariate statistics, and machine learning. J. Hydrol. 585, 124808.
Chousianitis, K., Del Gaudio, V., Sabatakakis, N., et al., 2016. Assessment of earthquake-induced landslide hazard in Greece: From Arias intensity to spatial distribution of slope resistance demand. Bull. Seismol. Soc. Am. 106 (1), 174–188. https://doi.org/10.1785/0120150172.
Corominas, J., van Westen, C., Frattini, P., Cascini, L., Malet, J.P., Fotopoulou, S., Catani, F., Van Den Eeckhaut, M., Mavrouli, O., Agliardi, F., Pitilakis, K., 2014. Recommendations for the quantitative analysis of landslide risk. Bull. Eng. Geol. Environ. 73, 209–263.
Das, S., 2019. Geospatial mapping of flood susceptibility and hydro-geomorphic response to the floods in Ulhas basin, India. Remote Sens. Appl. Soc. Environ. 14, 60–74.
Dikshit, A., Pradhan, B., 2021. Interpretable and explainable AI (XAI) model for spatial drought prediction. Sci. Total Environ. 801, 149797.
Dikshit, A., Pradhan, B., Alamri, A.M., 2021. Pathways and challenges of the application of artificial intelligence to geohazards modelling. Gondwana Res. 100, 290–301.
Dou, J., Yunus, A.P., Merghadi, A., Shirzadi, A., Nguyen, H., Hussain, Y., Avtar, R., Chen, Y., Pham, B.T., Yamagishi, H., 2020. Different sampling strategies for predicting landslide susceptibilities are deemed less consequential with deep learning. Sci. Total Environ. 720, 137320.
Downton, M.W., Miller, J.Z.B., Pielke Jr, R.A., 2005. Reanalysis of US National Weather Service flood loss database. Nat. Hazards Rev. 6, 13–22.
Eckstein, D., Künzel, V., Schäfer, L., 2021. Global Climate Risk Index 2021. Who Suff. Most from Extrem. Weather Events 2000–2019.
Fang, Z., Wang, Y., Peng, L., Hong, H., 2021. A comparative study of heterogeneous ensemble-learning techniques for landslide susceptibility mapping. Int. J. Geogr. Inf. Sci. 35, 321–347.
Fang, Z., Wang, Y., Peng, L., Hong, H., 2020. Integration of convolutional neural network and conventional machine learning classifiers for landslide susceptibility mapping. Comput. Geosci. 139, 104470.
Feizizadeh, B., Omarzadeh, D., Mohammadnejad, V., Khallaghi, H., Sharifi, A., Karkarg, B.G., 2022. An integrated approach of artificial intelligence and geoinformation techniques applied to forest fire risk modeling in Gachsaran, Iran. J. Environ. Plan. Manag., 1–23
Furlan, E., Torresan, S., Critto, A., Marcomini, A., 2018. Spatially explicit risk approach for multi-hazard assessment and management in marine environment: The case study of the Adriatic Sea. Sci. Total Environ. 618, 1008–1023.
Ghosh, A., Maiti, R., 2021. Soil erosion susceptibility assessment using logistic regression, decision tree and random forest: study on the Mayurakshi river basin of Eastern India. Environ. Earth Sci. 80, 1–16.
Goyes-Peñafiel, P., Hernandez-Rojas, A., 2021. Landslide susceptibility index based on the integration of logistic regression and weights of evidence: A case study in Popayan, Colombia. Eng Geol. 280, 105958.
Graham, O., Edwards, S., Robertson, R., 2022. Managing stakeholder relationships for improved situation awareness during volcanic emergencies: An Eastern Caribbean case study. Int. J. Disaster Risk Reduct. 67, 102656.
Habumugisha, J.M., Chen, N., Rahman, M., Islam, M.M., Ahmad, H., Elbeltagi, A., Sharma, G., Liza, S.N., Dewan, A., 2022. Landslide susceptibility mapping with deep learning algorithms. Sustainability 14, 1734.
Hosseini, F.S., Sigaroodi, S.K., Salajegheh, A., Moghaddamnia, A., Choubin, B., 2021. Towards a flood vulnerability assessment of watershed using integration of decision-making trial and evaluation laboratory, analytical network process, and fuzzy theories. Environ. Sci. Pollut. Res. 28, 62487–62498.
Hou, J., Zhou, N., Chen, G., Huang, M., Bai, G., 2021. Rapid forecasting of urban flood inundation using multiple machine learning models. Nat. Hazards 108, 2335–2356.
Huang, F., Cao, Z., Guo, J., Jiang, S.-H., Li, S., Guo, Z., 2020. Comparisons of heuristic, general statistical and machine learning models for landslide susceptibility prediction and mapping. Catena 191, 104580.
Hussain, M., Tayyab, M., Zhang, J., Shah, A.A., Ullah, K., Mehmood, U., Al-Shaibah, B., 2021. GIS-based multi-criteria approach for flood vulnerability assessment and mapping in district Shangla: Khyber Pakhtunkhwa, Pakistan. Sustainability 13, 3126.
Javidan, N., Kavian, A., Pourghasemi, H.R., Conoscenti, C., Jafarian, Z., Rodrigo-Comino, J., 2021. Evaluation of multi-hazard map produced using MaxEnt machine learning technique. Sci. Rep. 11, 1–20.
Jiang, P., Chen, J., 2016. Displacement prediction of landslide based on generalized regression neural networks with K-fold cross-validation. Neurocomputing 198, 40–47.
Kalantar, B., Ueda, N., Lay, U.S., Al-Najjar, H.A.H., Halin, A.A., 2019. Conditioning factors determination for landslide susceptibility mapping using support vector machine learning. In: IGARSS 2019-2019 IEEE International Geoscience and Remote Sensing Symposium. IEEE, pp. 9626–9629.
Kalantar, B., Ueda, N., Saeidi, V., Ahmadi, K., Halin, A.A., Shabani, F., 2020. Landslide susceptibility mapping: Machine and ensemble learning based on remote sensing big data. Remote Sens. 12, 1737.
Kappes, M.S., Keiler, M., Glade, T., 2010. From single-to multi-hazard risk analyses: a concept addressing emerging challenges.
Kappes, M.S., Keiler, M., von Elverfeldt, K., Glade, T., 2012. Challenges of analyzing multi-hazard risk: a review. Nat. Hazards 64, 1925–1958.
Karpouza, M., Chousianitis, K., Bathrellos, G.D., Skilodimou, H.D., Kaviris, G., Antonarakou, A., 2021. Hazard zonation mapping of earthquake-induced secondary effects using spatial multi-criteria analysis. Nat. Hazards 109, 637–669.
Khan, I., Lei, H., Shah, A.A., Khan, I., Muhammad, I., 2021. Climate change impact assessment, flood management, and mitigation strategies in Pakistan for sustainable future. Environ. Sci. Pollut. Res. 1–12.
Khosravi, K., Pourghasemi, H.R., Chapi, K., Bahri, M., 2016. Flash flood susceptibility analysis and its mapping using different bivariate models in Iran: a comparison between Shannon's entropy, statistical index, and weighting factor models. Environ. Monit. Assess. 188, 1–21.
Khosravi, K., Shahabi, H., Pham, B.T., Adamowski, J., Shirzadi, A., Pradhan, B., Dou, J., Ly, H.-B., Gróf, G., Ho, H.L., 2019. A comparative assessment of flood susceptibility modeling using multi-criteria decision-making analysis and machine learning methods. J. Hydrol. 573, 311–323.
Kritikos, T., Robinson, T.R., Davies, T.R.H., 2015. Regional coseismic landslide hazard assessment without historical landslide inventories: A new approach. J. Geophys. Res. Earth Surf. 120, 711–729.
LeCun, Y., Bengio, Y., Hinton, G., 2015. Deep learning. Nature 521, 436–444.
Li, Y., Chen, W., Rezaie, F., Rahmati, O., Davoudi Moghaddam, D., Tiefenbacher, J., Panahi, M., Lee, M.J., Kulakowski, D., Tien Bui, D., Lee, S., 2021. Debris flows modeling using geo-environmental factors: developing hybridized deep-learning algorithms. Geocarto Int., 1–25
Liu, Mei, Zhang, Yong, Shufeng, Tian, et al., 2020. Effects of loose deposits on debris flow processes in the Aizi Valley, southwest China. J. Mt. Sci. 17, 156–172. https://doi.org/10.1007/s11629-019-5388-9.
Lombardo, L., Tanyas, H., Nicu, I.C., 2020. Spatial modeling of multi-hazard threat to cultural heritage sites. Eng. Geol. 277, 105776.
Ma, L., Liu, Y., Zhang, X., Ye, Y., Yin, G., Johnson, B.A., 2019. Deep learning in remote sensing applications: A meta-analysis and review. ISPRS J. Photogramm. Remote Sens. 152, 166–177.
Mafi-Gholami, D., Zenner, E.K., Jaafari, A., Bakhtyari, H.R.R., Bui, D.T., 2019. Multi-hazards vulnerability assessment of southern coasts of Iran. J. Environ. Manage. 252, 109628.
Mallat, S., 2016. Understanding deep convolutional networks. Philos. Trans. R. Soc. A Math. Phys. Eng. Sci. 374. 20150203.
Mandal, K., Saha, S., Mandal, S., 2021. Applying deep learning and benchmark machine learning algorithms for landslide susceptibility modelling in Rorachu river basin of Sikkim Himalaya, India. Geosci. Front. 12, 101203.
Marin, G., Modica, M., Paleari, S., Zoboli, R., 2021. Assessing disaster risk by integrating natural and socio-economic dimensions: A decision-support tool. Socio-Econ. Plan. Sci. 77, 101032.
Marra, F., Destro, E., Nikolopoulos, E.I., Zoccatelli, D., Creutin, J.D., Guzzetti, F., Borga, M., 2017. Impact of rainfall spatial aggregation on the identification of debris flow occurrence thresholds. Hydrol. Earth Syst. Sci. 21, 4525–4532.
Merghadi, A., Yunus, A.P., Dou, J., Whiteley, J., ThaiPham, B., Bui, D.T., Avtar, R., Abderrahmane, B., 2020. Machine learning methods for landslide susceptibility studies: A comparative overview of algorithm performance. Earth-Sci. Rev. 207, 103225.
Mosavi, A., Golshan, M., Janizadeh, S., Choubin, B., Melesse, A.M., Dineva, A.A., 2020. Ensemble models of GLM, FDA, MARS, and RF for flood and erosion susceptibility mapping: a priority assessment of sub-basins. Geocarto Int., 1–20
Nachappa, T.G., Ghorbanzadeh, O., Gholamnia, K., Blaschke, T., 2020. Multi-hazard exposure mapping using machine learning for the State of Salzburg, Austria. Remote Sens. 12, 2757.
Nicodemus, K.K., 2011. Letter to the editor: On the stability and ranking of predictors from random forest variable importance measures. Brief. Bioinform. 12, 369–373.
Oh, H.J., Pradhan, B., 2011. Application of a neuro-fuzzy model to landslide-susceptibility mapping for shallow landslides in a tropical hilly area. Comput. Geosci. 37, 1264–1276.
Pham, V.D., Nguyen, Q.-H., Nguyen, H.-D., Pham, V.-M., Bui, Q.-T., 2020. Convolutional neural network—optimized moth flame algorithm for shallow landslide susceptible analysis. IEEE Access 8, 32727–32736.
Pourghasemi, H.R., Gayen, A., Edalat, M., Zarafshar, M., Tiefenbacher, J.P., 2020. Is multi-hazard mapping effective in assessing natural hazards and integrated watershed management? Geosci. Front. 11, 1203–1217.
Pourghasemi, H.R., Gayen, A., Panahi, M., Rezaie, F., Blaschke, T., 2019. Multi-hazard probability assessment and mapping in Iran. Sci. Total Environ. 692, 556–571.
Pourghasemi, H.R., Kerle, N., 2016. Random forests and evidential belief function-based landslide susceptibility assessment in Western Mazandaran Province, Iran. Environ. Earth Sci. 75, 185.
Pouyan, S., Pourghasemi, H.R., Bordbar, M., Rahmanian, S., Clague, J.J., 2021. A multi-hazard map-based flooding, gully erosion, forest fires, and earthquakes in Iran. Sci. Rep. 11, 1–19.
Rafiei-Sardooi, E., Azareh, A., Choubin, B., Mosavi, A.H., Clague, J.J., 2021. Evaluating urban flood risk using hybrid method of TOPSIS and machine learning. Int. J. Disaster Risk Reduct. 66, 102614.

Rahman, M., Chen, N., Elbeltagi, A., Islam, M.M., Alam, M., Pourghasemi, H.R., Tao, W., Zhang, J., Shufeng, T., Faiz, H., 2021. Application of stacking hybrid machine learning algorithms in delineating multi-type flooding in Bangladesh. J. Environ. Manage. 295, 113086.
Rahmati, O., Yousefi, S., Kalantari, Z., Uuemaa, E., Teimurian, T., Keesstra, S., Pham, T. D., Tien Bui, D., 2019. Multi-hazard exposure mapping using machine learning techniques: A case study from Iran. Remote Sens. 11, 1943.
Ranjbar, S., Hooshyar, M., Singh, A., Wang, D., 2018. Quantifying climatic controls on river network branching structure across scales. Water Resour. Res. 54, 7347–7360.
Sanam, K. Aksha, Lynn, M. Resler, Luke, Juran, et al., 2020. A geospatial analysis of multi-hazard risk in Dharan, Nepal. Geomatics, Natural Hazards and Risk 11 (1), 88–111. https://doi.org/10.1080/19475705.2019.1710580.
Segoni, S., Caleca, F., 2021. Definition of Environmental indicators for a fast estimation of landslide risk at National Scale. Land 10, 621.
Roy, J., Saha, S., 2019. Landslide susceptibility mapping using knowledge driven statistical models in Darjeeling District, West Bengal, India. Geoenviron. Disasters 6, 1–18.
Shaw, R., 2015. Disaster and climate change education in Pakistan, in: Disaster Risk Reduction Approaches in Pakistan. Springer, pp. 315–335.
Simard, P.Y., Steinkraus, D., Platt, J.C., 2003. Best Practices for Convolutional Neural Networks Applied to Visual Document Analysis. Icdar.
Simonyan, K., Zisserman, A., 2014. Very deep convolutional networks for large-scale image recognition. arXiv Prepr. arXiv1409.1556.
Skilodimou, H.D., Bathrellos, G.D., Chousianitis, K., Youssef, A.M., Pradhan, B., 2019. Multi-hazard assessment modeling via multi-criteria analysis and GIS: a case study. Environ. Earth Sci. 78, 47.
Song, J., Wang, Y., Fang, Z., Peng, L., Hong, H., 2020. Potential of ensemble learning to improve tree-based classifiers for landslide susceptibility mapping. IEEE J. Sel. Top. Appl. Earth Obs. Remote Sens. 13, 4642–4662.
Sun, Z., Sandoval, L., Crystal-Ornelas, R., Mousavi, S.M., Wang, J., Lin, C., Cristea, N., Tong, D., Carande, W.H., Ma, X., Rao, Y., 2022. A review of earth artificial intelligence. Comput. Geosci., 105034
Szegedy, C., Liu, W., Jia, Y., Sermanet, P., Reed, S., Anguelov, D., Erhan, D., Vanhoucke, V., Rabinovich, A., 2015. Going deeper with convolutions. In: Proceedings of the IEEE Conference on Computer Vision and Pattern Recognition, pp. 1–9.
Tehrany, M.S., Pradhan, B., Jebur, M.N., 2015. Flood susceptibility analysis and its verification using a novel ensemble support vector machine and frequency ratio method. Stoch. Environ. Res. Risk Assess. 29, 1149–1165.
Uitto, J.I., Shaw, R., 2016. Sustainable development and disaster risk reduction: Introduction, in: Sustainable Development and Disaster Risk Reduction. Springer, pp. 1–12.
Ullah, F., Saqib, S.E., Ahmad, M.M., Fadlallah, M.A., 2020. Flood risk perception and its determinants among rural households in two communities in Khyber Pakhtunkhwa, Pakistan. Nat. Hazards 104, 225–247.
Ullah, K., Zhang, J., 2020. GIS-based flood hazard mapping using relative frequency ratio method: A case study of Panjkora River Basin, eastern Hindu Kush, Pakistan. PLoS One 15, e0229153.
UN, 2002. Johannesburg Plan of Implementation of the World Summit on Sustainable Development. United Nations. Technical Report.
UNEP, 1992. Agenda 21.Tech. rep., United Nations Environment Programme. http://www. un.org/esa/dsd/agenda21/res_agenda21_07.shtml, Accessed on: 3 September 2009.
Wang, Y., Fang, Z., Hong, H., 2019. Comparison of convolutional neural networks for landslide susceptibility mapping in Yanshan County, China. Sci. Total Environ. 666, 975–993.
Wang, Y., Fang, Z., Hong, H., Peng, L., 2020a. Flood susceptibility mapping using convolutional neural network frameworks. J. Hydrol. 582, 124482.
Wang, Y., Fang, Z., Wang, M., Peng, L., Hong, H., 2020b. Comparative study of landslide susceptibility mapping with different recurrent neural networks. Comput. Geosci. 138, 104445.
Wasson, R.J., 1978. A debris flow at Reshūn, Pakistan Hindu Kush. Geogr. Ann. Ser. A, Phys. Geogr. 60, 151–159.
Wu, S., Chen, J., Zhou, W., Iqbal, J., Yao, L., 2019. A modified Logit model for assessment and validation of debris-flow susceptibility. Bull. Eng. Geol. Environ. 78, 4421–4438.
Yamashita, R., Nishio, M., Do, R.K.G., Togashi, K., 2018. Convolutional neural networks: an overview and application in radiology. Insights Imag. 9, 611–629.
Yanar, T., Kocaman, S., Gokceoglu, C., 2020. Use of Mamdani fuzzy algorithm for multi-hazard susceptibility assessment in a developing urban settlement (Mamak, Ankara, Turkey). ISPRS Int. J. Geo-Inf. 9, 114.
Yariyan, P., Omidvar, E., Minaei, F., Ali Abbaspour, R., Tiefenbacher, J.P., 2022. An optimization on machine learning algorithms for mapping snow avalanche susceptibility. Nat. Hazards 111, 79–114.
Yi, Y., Zhang, Z., Zhang, W., Jia, H., Zhang, J., 2020. Landslide susceptibility mapping using multiscale sampling strategy and convolutional neural network: A case study in Jiuzhaigou region. Catena 195, 104851.
Youssef, A.M., Pradhan, B., Dikshit, A., Al-Katheri, M.M., Matar, S.S., Mahdi, A.M., 2022a. Landslide susceptibility mapping using CNN-1D and 2D deep learning algorithms: comparison of their performance at Asir Region, KSA. Bull. Eng. Geol. Environ. 81, 1–22.
Youssef, A.M., Pradhan, B., Dikshit, A., Mahdi, A.M., 2022b. Comparative study of convolutional neural network (CNN) and support vector machine (SVM) for flood susceptibility mapping: a case study at Ras Gharib, Red Sea. Geocarto Int., 1–26
Yousefi, S., Pourghasemi, H.R., Emami, S.N., Pouyan, S., Eskandari, S., Tiefenbacher, J. P., 2020. A machine learning framework for multi-hazards modeling and mapping in a mountainous area. Sci. Rep. 10, 1–14.
Zêzere, J.L., Pereira, S., Melo, R., et al., 2017. Mapping landslide susceptibility using data-driven methods. Sci. Total Environ. 589 (1), 250–267. https://doi.org/10.1016/j.scitotenv.2017.02.188.
Zhang, G., Wang, M., Liu, K., 2019. Forest fire susceptibility modeling using a convolutional neural network for Yunnan province of China. Int. J. Disaster Risk Sci. 10, 386–403.
Zhao, G., Pang, B., Xu, Z., Peng, D., Zuo, D., 2020. Urban flood susceptibility assessment based on convolutional neural networks. J. Hydrol. 590, 125235.